J. Synchrotron Rad. (1998). **5**, 952–954

X-ray characterization of α-Fe_2O_3 single crystals containing 2.2% and 95% ^{57}Fe

J. Y. Zhao,[a]* X.-W. Zhang,[a] M. Ando,[a] Y. Yoda,[b] S. Kikuta[b] and H. Takei[c]

[a]Institute of Materials Structure Science, High Energy Accelerator Research Organization, Oho 1-1, Tsukuba, Ibaraki 305, Japan, [b]Department of Applied Physics, Faculty of Engineering, University of Tokyo, Hongo, Bunkyo-ku, Tokyo 113, Japan, and [c]Department of Earth and Space Science, Faculty of Science, Osaka University, Machikaneyama 1-16, Toyonaka, Osaka 560, Japan. E-mail: jiyong@kekvax.kek.jp

(*Received 4 August 1997; accepted 10 November 1997*)

α-Fe_2O_3 single crystals containing 2.2% and 95% ^{57}Fe isotopes were characterized by means of X-ray topography, the diffraction rocking curve and the integrated intensity. These crystals were revealed to be nearly perfect and suitable for a further nuclear-resonant Bragg-scattering study.

Keywords: hematite; single crystals; X-ray topography; rocking curves; integrated intensity.

1. Introduction

Nuclear-resonant Bragg scattering (NBS) of hematite (α-Fe_2O_3) single crystals containing ^{57}Fe isotopes has been studied for many years by means of the conventional Mössbauer method. With improved growth techniques of the flux method, highly perfect hematite crystals containing ^{57}Fe enriched to 95% are now available. Their size ranges up to 10 mm × 10 mm. Their crystallographic quality has been characterized by means of X-ray topography by Suzuki *et al.* (1992). As pointed out by Zhao (1995), the crystal lattice occupied by the non-resonant isotopes ^{56}Fe in hematite can be regarded as 'nuclear point defects' in the crystal from the viewpoint of NBS. In order to see the basic X-ray diffraction phenomenon in hematite single crystals with various isotopic contents, nearly perfect crystals are needed. For this study, hematite single crystals with two kinds of ^{57}Fe abundance, one 2.2% and the other 95%, have been successfully grown. Their imperfections have been characterized by X-ray topography, the X-ray rocking curve and the integrated intensity. In this paper, detailed results of their X-ray characterization are described.

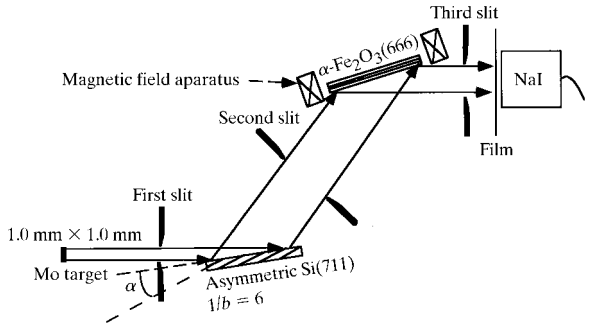

Figure 1
Schematic set-up of the double-crystal diffraction geometry. The X-ray came from an Mo target. The monochromator was an asymmetric Si(711) double crystal with $\alpha = 20.2^\circ$ and asymmetric factor $1/b = 6$. An external magnetic field was applied to the sample in the diffraction plane.

2. X-ray topography and rocking-curve measurement

The as-grown crystal surface of a hematite single crystal is a $(111)_r$ plane, where the subscript r indicates rhombohedral symmetry. The crystal surface exposed to air during growth was smooth and shining, whereas the opposite side which contacted with the flux was lusterless and rough. The smooth surface was used in our experiment without further polishing. The two crystal samples used in this experiment are the naturally abundant one with 2.2% ^{57}Fe and 4 × 6 × 0.5 mm in size (referred to as $S_{2.2}$) and the enriched one with 95% ^{57}Fe and 5 × 6 × 0.5 mm in size (referred to as S_{95}).

The experimental set-up for the double-crystal X-ray topography and rocking-curve measurement is shown in Fig. 1. A laboratory X-ray generator (18 kW) was used and its apparent X-ray source size from an Mo target was 1.0 mm × 1.0 mm. X-rays were monochromated and collimated by an asymmetric reflection of Si 711 so as to form an almost non-dispersive (+,−) setting with hematite $(666)_r$ planes, where the difference between their lattice spacings, $\Delta d/d$, is 0.26%. An expanded monochromatic beam for taking topographs was obtained after the Si 711 asymmetric diffraction, where the angle between the Bragg plane and the crystal surface $\alpha = 20.2^\circ$ and the asymmetric factor $1/b = 6$. Since the magnetic domain in hematite can be aligned into a single domain state (Nathans *et al.*, 1964), an external magnetic field of 1 kGauss, sufficient to saturate the domain in the sample, was applied during the experiment. The X-ray topographs were

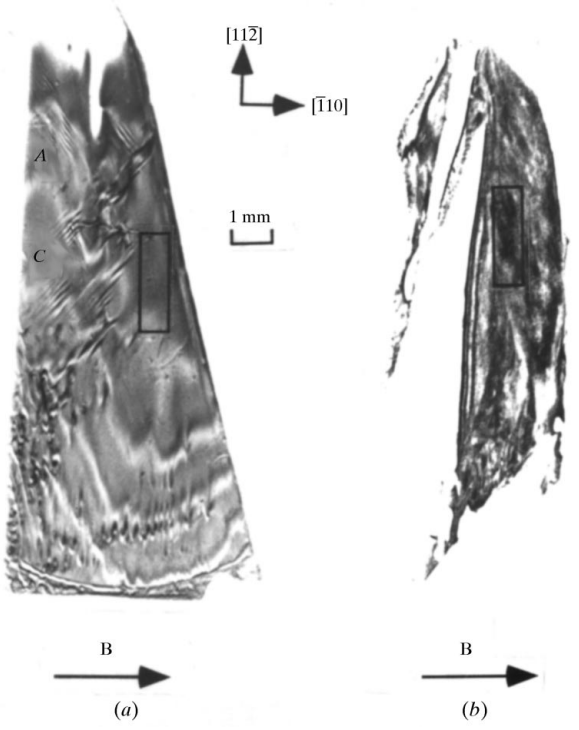

Figure 2
The multi-exposure X-ray topographs of the 666 reflection taken with Mo $K\alpha_1$ of samples (*a*) S_{95} and (*b*) $S_{2.2}$. The scanning angular step was $\Delta\theta$ = 4.5 arcsec. The topographs were recorded on Ilford L4 nuclear plates, with 30 min for each exposure and 2.5 h exposure time in total, by the generator operated at 55 kV, 240 mA.

Table 1
Extinction distance (l_{ext}), absorption depth (l_{abs}) and integrated reflection of S_{22} for 032 Å.

The diffractions are (*hhh*), with *h* listed in the left-hand column. R_D, R_K are theoretical values of the dynamical theory and the kinematical theory, respectively. θ_B is the Bragg angle, and P is the polarization factor, $P = \cos(2\theta_B)$. $R_{2.2}$ is the measured integrated reflection.

h	l_{ext} (μm)	l_{abs} (mm)	R_D ($\times 10^{-7}$)	$R_D \sin(2\theta_B)/P$ ($\times 10^{-7}$)	R_K ($\times 10^{-7}$)	$R_K \sin(2\theta_B)/P$ ($\times 10^{-7}$)	$R_{2.2}$ ($\times 10^{-7}$)	$R_{2.2}$ ($\times 10^{-7}$)
6	3.3	1.3	9.7	4.4	1300	585	14.50 ± 0.05	6.58 ± 0.02
8	9.1	1.8	5.1	3.3	350	227	7.98 ± 0.08	5.13 ± 0.05
10	12	2.3	5.4	4.8	410	358	7.3 ± 0.1	6.4 ± 0.1
12	36	2.7	2.3	2.7	890	105	2.3 ± 0.2	2.8 ± 0.2

recorded on nuclear plates (Ilford L4) or X-ray film (Fuji 80). The measured topographs and rocking curves are shown in Figs. 2 and 3, respectively.

Since a topograph taken at each different position of a rocking curve showed only part of the sample, the whole view of the sample was obtained by a multi-exposure in double-crystal topography, as shown in Fig. 2, while changing the angle of the sample along its rocking-curve profile by a step of 4.5 arcsec. The exposure time for each was 30 min while the X-ray generator was running at 55 kV and 240 mA. The indices in Fig. 2 are expressed by hexagonal symmetry. The 'zebra' contour lines in Fig. 2(*a*) correspond to the scanning step. The radius of curvature of S_{95} could have been estimated from these separate lines. The more precise radius was determined by measuring the peak shift of the rocking curve while scanning a narrow silt (0.1 mm × 0.1 mm) across the monochromatic beam whose size was about 6 mm (H) × 10 mm (V). The bending radii of the diffraction plane of the selected areas, marked with a rectangle in Figs. 2(*a*) and 2(*b*), in the samples S_{95} and $S_{2.2}$ were determined as approximately 113 m and 39 m, respectively. In the *A* and *C* regions in Fig. 2(*a*), black and white fine striations along the $\langle 0\bar{1}1\rangle_h$ and $\langle 10\bar{1}\rangle_h$ directions are found intersecting [110] at 45°, while no such contrast was found along the $\langle \bar{1}10\rangle_h$ direction. Such contrast is presently under study. In Fig. 2(*b*) the grain structure of $S_{2.2}$ could be found, and the largest grain was selected for the rocking-curve measurement. The areas in the rectangular mark correspond to the selected regions where the rocking curves of $S_{95}(n)$ and $S_{2.2}(n)$ in Fig. 3 were taken.

Fig. 3 shows the measured rocking curves of S_{95} and $S_{2.2}$. Broken and solid lines correspond to those taken when the second slit in Fig. 1 is fully open or closed to 0.3 × 1.0 mm in size, respectively. The FWHMs in units of arcsec are labelled in the figure. The calculated value of the FWHM by convolution of hematite 666 and Si 711 is 0.68 arcsec. When the X-ray beam illuminates the whole sample region, the widths of the rocking curves $S_{95}(w)$ and $S_{2.2}(w)$ become wider as they are comprised of several grains. When the slit was closed, sharper and narrower rocking curves $S_{95}(n)$ and $S_{2.2}(n)$ were obtained as shown in Figs. 3(*a*) and 3(*b*). Their associated FWHMs were 1.5 arcsec and 5.0 arcsec; the deconvoluted FWHMs considering the bending effect were 0.9 arcsec and 3.5 arcsec, respectively.

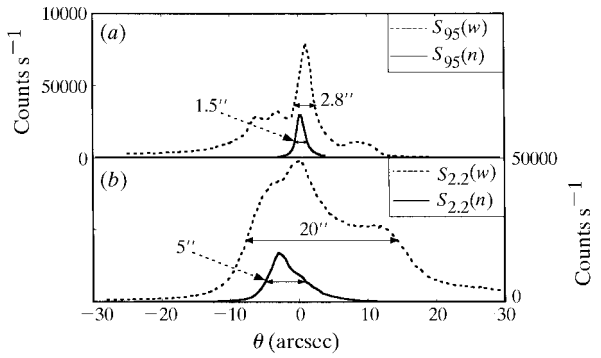

Figure 3
Measured rocking curves of the samples of (*a*) S_{95} and (*b*) $S_{2.2}$. $S_{95}(w)$ and $S_{2.2}(w)$ represent the curves when the second slit was opened widely, when the whole sample area was illuminated by the incident beam. $S_{95}(n)$ and $S_{2.2}(n)$ represent the curve when the second slit was 0.3 mm × 1.0 mm. The source condition was 50 kV, 50 mA for $S_{95}(w)$, 50 kV, 200 mA for $S_{95}(n)$ and 50 kV, 100 mA for $S_{2.2}(w)$ and $S_{2.2}(n)$.

It can be found from the above measurement that even the present crystal samples contain defects, such as bending and grains; they are highly perfect in some selected areas of the samples.

3. Integrated intensity

In early X-ray diffraction work, the integrated intensity of crystals with different degrees of imperfection has been used to verify the theoretical formulae of the dynamical and kinematical theories (Compton, 1917; Bragg, 1921; James, 1948). Following Zachariasen (1967) and Schneider (1977), if the integrated reflection R equals R_D for the dynamical theory applied to a defect-free crystal whose thickness is much larger than the extinction distance, the crystal can be called ideally perfect; if R equals R_K for the kinematical theory, it can be called ideally imperfect. According to the theories, R_D and R_K depend on the structure factor of a unit cell, the X-ray wavelength, the polarization factor and the absorption. For an actual crystal, the integrated intensity should lie between these two extremes. In the case of a hematite crystal, the absorption for Mo $K\alpha_1$ radiation is relatively large and no large difference between R_D and R_K can be found. From the viewpoint of experimental clarity, using X-rays with $\lambda = 0.32$ Å is much more preferable because the absorption of a hematite crystal is relatively weak ($\mu_l = 1.55$ cm^{-1}) and then the difference of the integrated reflection between R_D and R_K is great, R_K/R_D ranging from one to three orders.

Fig. 4 shows the experimental set-up for the integrated intensity measurement at bending-magnet beamline NE5 at AR, KEK. A double-crystal Si(111) monochromator was used during the measurement. The diffraction plane of the sample was perpendicular to the Si(111) diffraction plane; the polarization factor was

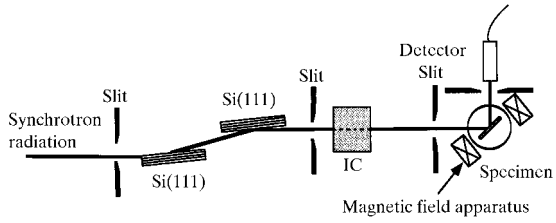

Figure 4
Experimental setting of the integrated intensity measurement at AR-NE5, KEK. IC is the ion chamber. The detector was a PIN-photodiode.

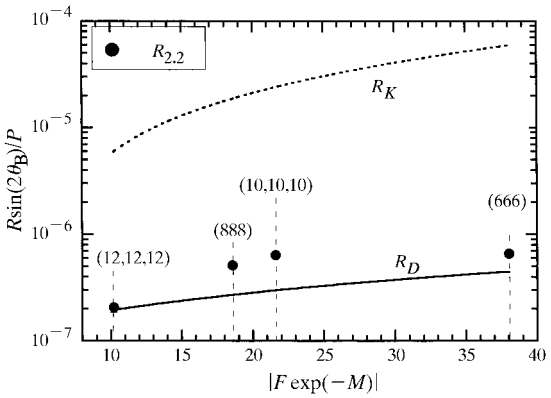

Figure 5
Integrated reflection of $S_{2.2}$ measured with $\lambda = 0.32$ Å. The abscissae are the structure factors. The coordinates are the products of the integrated reflection and sin $(2\theta_B)$ and divided by the polarization factor P, where θ_B is the Bragg angle. The solid line R_D and the dashed line R_K are theoretical calculations in the frame of the dynamical and kinematical theories, respectively.

then $P = \cos(2\theta_B)$, where θ_B is the diffraction Bragg angle of the sample. An ion chamber, IC, was used to monitor the intensity of the incident beam. The integrated reflection of sample $S_{2.2}$ was measured and the results are shown in Fig. 5, where the $(hhh)_r$ reflections with $h = 6$, 8, 10 and 12 were measured. The abscissae here are the structure factors corrected by the Debye–Waller factor, the coordinates are the products of the integrated reflection and the geometric factor $\sin 2\theta_B$ and divided by the polarization factor P. The dotted line R_K and the solid line R_D are for an ideally imperfect crystal and perfect crystal given by the standard kinematical and dynamical diffraction theories (*e.g.* James, 1948; Pinsker, 1978), respectively. The measured integrated reflection $R_{2.2}$ is shown as the solid circles and the diffraction indices are labelled in the figure. The measured and theoretical integrated reflection, the extinction distance and absorption depth are listed in Table 1.

The extinction distance l_{ext} and the absorption depth l_{abs} in the Bragg case are defined as (Kikuta, 1992)

$$l_{ext} = v_c \sin\theta_B / \left[2|P| r_e \lambda |F_{hkl}| \exp(-M)\right], \quad (1)$$

$$l_{abs} = \sin\theta_B / \mu_l, \quad (2)$$

where v_c is the volume of the unit cell, θ_B is the Bragg angle, P is the polarization factor, r_e is the classical electron radius, λ is the wavelength, F_{hkl} is the crystal structure factor, M is the Debye–Waller factor and μ_l is the linear absorption coefficient.

It can be found from Fig. 5 and Table 1 that the theoretical curves R_K and R_D are different by two orders due to the difference of the extinction distance and absorption depth. The sample $S_{2.2}$ was found to be obviously quite perfect because its integrated reflection $R_{2.2}$ lies nearer to the R_D curve, but differs greatly from the R_K curve. This reveals that the effective reflection depth of this sample is almost equal to the extinction distance, as shown in Table 1, much smaller than the absorption depth or the sample thickness (500 μm). This suggests that a dynamical diffraction wave field is formed in quite a thin layer in this sample.

4. Conclusions

Two hematite single crystals containing ^{57}Fe of 2.2% and 95% are characterized by X-ray topography, the rocking curve and the integrated intensity. The results show that the diffraction widths of the present samples are quite narrow and relatively close to their intrinsic width; the integrated reflection of $S_{2.2}$ is close to a dynamical diffraction case for $\lambda = 0.32$ Å. It has been revealed that the crystals contain defects such as bending defects and those formed by grains; selected grains were found to be highly perfect and therefore suitable for further NBS measurements.

We would like to thank Dr K. Hyodo for his help during the experiment at AR-NE5. This work was supported in part by a Grant-in-Aid for Specially Promoted Research and a Grant-in-Aid for JSPS fellows from the Ministry of Education, Science, Culture and Sports, Japan.

References

Bragg., W. H. (1921). *Proc. Phys. Soc. London*, **33**, 304.
Compton, A. H. (1917). *Phys. Rev.* **9**, 29.
James, R. W. (1948). *The Optical Principles of the Diffraction of X-rays*, pp. 27–90. London: Bell.
Kikuta, S. (1992). *X-ray Diffraction and Scattering.* University of Tokyo Press.
Nathans, R., Pickart, S. J., Alperin, H. A. & Brown, P. J. (1964). *Phys. Rev. A*, **136**, 1641–1647.
Pinsker, Z. G. (1978). *Dynamical Scattering of X-rays in Crystals*, pp. 274–277. Berlin: Springer-Verlag.
Schneider, J. R. (1977). *Acta Cryst.* A**33**, 235–243.
Suzuki, C. K., Ohno, H., Takei, H., Sakai, F., Yoda, Y., Kudo, Y., Izumi, K., Ishikawa, T., Kikuta, S., Zhang, X. W., Matsushita, T. & Ando, M. (1992). *Rev. Sci. Instum.* **63**, 1206.
Zachariasen, W. H. (1967). *Acta Cryst.* **23**, 558–564.
Zhao, J. Y. (1995). PhD thesis, The Graduate University for Advanced Studies, Japan.